

Regulated tissue fluidity steers zebrafish body elongation

Andrew K. Lawton¹, Amitabha Nandi¹, Michael J. Stulberg¹, Nicolas Dray¹, Michael W. Sneddon², William Pontius³, Thierry Emonet^{1,2,3} and Scott A. Holley^{1,*}

SUMMARY

The tailbud is the posterior leading edge of the growing vertebrate embryo and consists of motile progenitors of the axial skeleton, musculature and spinal cord. We measure the 3D cell flow field of the zebrafish tailbud and identify changes in tissue fluidity revealed by reductions in the coherence of cell motion without alteration of cell velocities. We find a directed posterior flow wherein the polarization between individual cell motion is high, reflecting ordered collective migration. At the posterior tip of the tailbud, this flow makes sharp bilateral turns facilitated by extensive cell mixing due to increased directional variability of individual cell motions. Inhibition of Wnt or Fgf signaling or *cadherin 2* function reduces the coherence of the flow but has different consequences for trunk and tail extension. Modeling and additional data analyses suggest that the balance between the coherence and rate of cell flow determines whether body elongation is linear or whether congestion forms within the flow and the body axis becomes contorted.

KEY WORDS: Zebrafish, Tailbud, Body elongation, Cell migration

INTRODUCTION

Vertebrate axis elongation intertwines cell migration, cell differentiation and tissue patterning within a structure called the tailbud. The tailbud is the posterior end of the growing trunk and tail and contains both neural and mesodermal anlagen (Griffith et al., 1992; Holmdahl, 1925; Wilson et al., 2009). Genetic and fate-mapping studies demonstrate the existence of a population of bipotential neural/mesodermal stem cells in the mouse and zebrafish tailbud (Martin and Kimelman, 2012; Takemoto et al., 2011; Tzouanacou et al., 2009). Inhibition of cell division during gastrulation and/or the segmentation period modestly reduces body length, suggesting that cell migration primarily drives elongation (Harrington et al., 2010; Quesada-Hernández et al., 2010; Zhang et al., 2008). In zebrafish, cell-labeling and cell-tracking experiments have elucidated the spatiotemporal patterns of cell movement and cell division in the blastula, gastrula and early tailbud (Kanki and Ho, 1997; Keller et al., 2008; Olivier et al., 2010).

Within the tailbud, cell differentiation, axis elongation and segmentation are linked by Fibroblast growth factor (Fgf) and canonical/ β -catenin-dependent Wnt signaling (Kimelman, 2006; Pourquié, 2011). Abrogation of canonical Wnt signaling in mouse or zebrafish leads to axis truncation as Wnt is involved in specifying and maintaining mesodermal progenitors (Dunty et al., 2008; Martin and Kimelman, 2008; Martin and Kimelman, 2012; Shimizu et al., 2005; Szeto and Kimelman, 2004; Takada et al., 1994; Thorpe et al., 2005). The roles of Fgf signaling in trunk and tail development have been studied by genetic perturbation and chemical inhibition of Fgf receptors (Fgfrs) with SU5402 (Draper et al., 2003; Dubrulle et al., 2001; Mathis et al., 2001; Mohammadi et al., 1997; Naiche et al., 2011; Niwa et al., 2007; Sawada et al., 2001; Sun et al., 1999; Wahl et al., 2007). Conditional knockout (cKO) of Fgfr1 or Fgf4 and Fgf8 in the mouse mesoderm leads to

axis truncation accompanied by a reduction in mesoderm differentiation (Naiche et al., 2011; Niwa et al., 2007; Wahl et al., 2007). In zebrafish, short and/or bent embryos are commonly caused by mutation or overexpression of cell signaling and adhesion genes, but the mechanics of such defects are poorly understood (Draper et al., 2001; Flowers et al., 2012; Hammerschmidt et al., 1996; Jülich et al., 2005; Kawamura et al., 2008; Keegan et al., 2002; Lele et al., 2002; Marlow et al., 2004; Okuda et al., 2010; Rauch et al., 1997a; Row and Kimelman, 2009; Shimizu et al., 2005; Stoick-Cooper et al., 2007; Tucker et al., 2008; Weidinger et al., 2005; Zhang et al., 2006).

Fgf and canonical Wnt signaling form a network with T-box family transcription factors to govern cell fates within the tailbud (Kimelman, 2006; Wilson et al., 2009). In zebrafish, four T-box genes, *ntla*, *ntl*, *spt* and *tbx6*, function in combination to specify axial and paraxial mesoderm (Amacher and Kimmel, 1998; Griffin et al., 1998; Griffin and Kimelman, 2002; Griffin and Kimelman, 2003; Martin and Kimelman, 2008). *ntl* and *spt* also upregulate transcription of Fgf genes, which, in turn, promote T-box gene transcription, forming a positive autoregulatory loop that is required for mesoderm development in the tailbud (Draper et al., 2003; Griffin et al., 1998; Griffin and Kimelman, 2003). Recent data suggest that the T-box-Fgf loop is restricted to the axial mesoderm whereas another positive feedback loop comprising *ntl*, *bra* and canonical Wnt signaling specifies and maintains paraxial mesoderm precursors (Martin and Kimelman, 2008).

Non-canonical/planar cell polarity Wnt signaling and Fgf signaling may directly and/or indirectly regulate cell migration within the tailbud. A recent study found that Fgf signaling promotes high cell motility in the chick tailbud (Bénazéraf et al., 2010). In the primitive streak, there is evidence that Fgf4 functions as a chemoattractant whereas Fgf8b acts as a chemorepellant (Yang et al., 2002). In the chick dermomyotome, Fgf8 can act as a chemoattractant to motor neurons in a process mediated by Fgfr1 (Shirasaki et al., 2006). The chemotactic property of Fgf ligands is best documented in the process of branching morphogenesis in the *Drosophila* tracheal system (Affolter et al., 2009; Sutherland et al., 1996). Similarly, *in vitro* data suggest that Fgf10 might serve as a chemoattractant in branching morphogenesis of the mouse lung

¹Department of Molecular, Cellular and Developmental Biology, ²Interdepartmental Program in Computational Biology and Bioinformatics, ³Department of Physics, Yale University, New Haven, CT 06520, USA.

*Author for correspondence (scott.holley@yale.edu)

(Park et al., 1998). During gastrulation, the role of the non-canonical Wnt pathway in regulating cell migration during convergence extension has been extensively studied (Heisenberg and Solnica-Krezel, 2008). The non-canonical Wnt pathway establishes cell polarity, which is necessary for efficient mesoderm migration towards the dorsal midline (Roszko et al., 2009; Wallingford et al., 2002). Non-canonical Wnt signaling is also required for zebrafish trunk and tail elongation (Marlow et al., 2004; Rauch et al., 1997b; Zhang et al., 2006).

Here, we measured the cell flow field within the zebrafish tailbud during trunk elongation. We combine live zebrafish imaging, cell tracking and metrics from fluid mechanics and condensed matter physics to quantify the three-dimensional (3D) cell velocity field along the posterior leading edge of the zebrafish embryo. We identify a transition in tissue fluidity revealed as a decrease in the global order of the cell flow in the absence of corresponding changes in cell velocity. We quantify the changes in the cell flow due to moderate abrogation of Wnt and Fgf signaling. Computer simulations suggest that a decrease in the coherence of collective migration combined with a normal flow rate leads to a ‘traffic jam’ in the posterior tailbud that, when resolved, can lead to a severely contorted trunk. By contrast, when the decrease in coherence of collective migration is accompanied by a reduction in the flow, only a modest reduction in axial growth is observed and morphological ‘kinks’ are restricted to the tip of the tail. These data suggest that the flow rate and coherence of the collective migration within the tailbud must be balanced for linear elongation of the developing vertebrate trunk.

MATERIALS AND METHODS

Zebrafish methods

Zebrafish were raised according to standard Institutional Animal Care and Use Committee approved protocols (Nüsslein-Volhard and Dahm, 2002). The *pac^{101B}* allele of *cdh2* and TLF were used (Lele et al., 2002). Heat shock of the *hsΔTCF-GFP* transgenic line (Lewis et al., 2004) was carried out as described (Stoick-Cooper et al., 2007; Weidinger et al., 2005). Tailbud dissections and qPCR were performed as previously detailed (Stulberg et al., 2012). Two-photon laser uncaging of caged fluorescein dextran was performed as described (Russek-Blum et al., 2010).

Analysis of cell motion

One-cell-stage wild-type embryos were injected with *nuclear localization signal red fluorescent protein (nlsRFP)* mRNA (70 ng/μl) or both *nlsRFP* (70 ng/μl) and *notum1a* (100 ng/μl) mRNAs. At the ten-somite stage, embryos were mounted in low-melt agarose and imaged using a Zeiss LSM 350 confocal microscope. All time-lapses were taken at 18°C using a Linkam Scientific PE100 stage. Image stacks were taken with an interval of 2.5–3.5 minutes. We imaged four wild-type embryos, six *notum1a* overexpressing embryos and six embryos treated for 3 hours beginning at the tailbud stage with 50 μM SU5402. Cell tracking was performed using Imaris (Bitplane).

Double-labeled cells were used to calculate tracking accuracy. Embryos were injected with *nlsRFP* mRNA at the one-cell stage and with *nlsGFP* mRNA (70 ng/μl) at the eight-cell stage. Four-dimensional (4D) imaging was performed and red and green channels were independently tracked. If the red track of a double-labeled cell jumped to another cell during the time lapse then the track was scored as an ‘error’. If the track ended prematurely or if the track was split into two tracks they were scored as ‘split’. If the track had no jumps or splits and followed the cell completely it was scored as ‘complete’. Among 222 double-labeled cells in three embryos, 15% (33/222) contained an error, 51% (113/222) of the tracks were ‘split’ and 34% (76/222) of the tracks were ‘complete’.

Quantitative analysis of cell motion

Imaris software (Bitplane) was used to track the 3D position of individual nuclei and extract basic statistics of motion. Before we started the analysis,

the cell-position data for the entire tailbud was divided into different regions, namely the dorsal medial zone (DM; red), the progenitor zone (PZ; green) and the presomitic mesoderm (PSM; blue). This subdivision was carried out manually in Imaris by sorting tracks by physical location. Mean track speed, coefficient of variation and track straightness were calculated using Imaris. The display of the tracks in the top 10% displacement was also performed by Imaris. All other analyses of the cell track data and computer modeling of the cell flow were performed using custom MatLab routines as detailed in supplementary material Appendix S1.

RESULTS

Discrete regions of the tailbud exhibit unique patterns of cell flow

Using 4D confocal imaging and cell tracking, we examined the cell flow of the paraxial mesoderm and its progenitors during trunk elongation (Fig. 1A). We divided the tracks into three tailbud regions based on morphology and patterns of gene expression. The dorsal medial zone (DM) lies in the posterior tailbud dorsal to the axial and paraxial mesoderm (Fig. 1C,D, red domain) and contains recently identified bipotential neural/mesodermal stem cells (Martin and Kimelman, 2012). The DM lacks expression of mesoderm and segmentation genes, such as *tbx6* and *her1* (Griffin et al., 1998; Holley et al., 2000). The progenitor zone (PZ) is ventral to the DM and posterior to the notochord (Fig. 1C,D, green domain) and exhibits *tbx6* and *her1* transcription. The presomitic mesoderm (PSM) consists of two bilateral columns of cells (Fig. 1C,D, cyan domains) that display the *her1* stripes created by the segmentation clock (Holley et al., 2000; Pourquié, 2011). The PSM is covered with an extracellular matrix that separates it from the overlying DM and adjacent axial mesoderm (Jülich et al., 2009). Generally, the PSM exhibits much less cell movement than does the posterior tailbud (Mara et al., 2007).

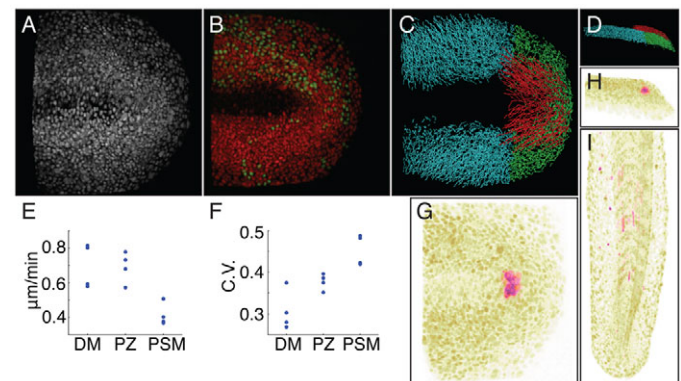


Fig. 1. Cell movement in the wild-type zebrafish tailbud.

(A) Confocal image stacks of RFP-labeled nuclei were taken through time and nuclei were tracked in 4D. (B) Independent tracking of red and green double-labeled nuclei revealed cell tracking to be 85% accurate. (C) Cell tracks were divided into regions of interest: dorsal medial zone (DM; red), progenitor zone, (PZ; green), presomitic mesoderm (PSM; cyan). (D) A lateral view of the image shown in C. (E) Examination of mean track speeds. *P*-values calculated using ANOVA with additional validation by permutation tests. The DM and PZ speeds are equivalent (DM vs PZ, $P > 0.05$) and are higher than PSM (DM vs PSM, $P < 0.05$; PZ vs PSM, $P < 0.05$). (F) The means of the coefficient of variation (CV) of track speed show that the CV increases from the DM to PZ ($P < 0.05$) and from the PZ to PSM ($P < 0.05$). (G–I) Two-photon labeling of DM cells at the ten-somite stage. (G) Dorsal view. (H) Lateral view. (I) After completing elongation, the uncaged cells differentiated as myofibers. A–C and G are dorsal views. In all panels, anterior is left the right except panel I in which anterior is up.

We found the cell tracking to be 85% accurate over the 2.5-3 hour dataset (Fig. 1B; Materials and methods) and utilized the cell tracks to examine the general patterns of movement in the tailbud including track straightness, mean speed and coefficient of variation (CV; standard deviation divided by the mean) of the speed (Fig. 1E,F; supplementary material Fig. S1A-D; Fig. S2A-D). Independent fate mapping was used to define the longer-term flow of cells during trunk growth. We labeled clusters of approximately five cells in the DM by two-photon uncaging of caged fluorescein at the ten-somite stage (Fig. 1G,H) and allowed the embryos to complete body elongation (Fig. 1I). Of 13 embryos, ten exhibited labeled myofibers, indicating that DM cells migrated through the PZ to the PSM and were incorporated into somites. The separation of the myofibers by up to eight somites indicates that the labeled cells resided in the PZ for different lengths of time and entered the PSM up to 3-4 hours apart.

Utilizing the raw cell track data, we compared the statistics of cell motion in the DM, PZ and PSM. Cell movement within the DM was rapid, showed low CV and exhibited the straightest trajectories (Fig. 1E,F; supplementary material Fig. S1A-D, Fig. S2A-D). PZ cell movement was equally rapid, but displayed greater CV of track speed and reduced ‘straightness’ relative to the DM. The PSM mean speed was much diminished, had high CV of track speed and the tracks were the least straight.

These changes in cell motion are visualized with a vector map in which the 3D cell velocities are projected onto the two-dimensional (2D) x and y planes and averaged over $10 \mu\text{m}^2$ sectors and in the z direction (Fig. 2A). Movement within each sector is averaged for the length of the movie with speed indicated by heat map and projected velocity by arrow orientation and length. The vector maps show the rapid cell movement in the posterior tailbud and the gradual decrease in motion in the PSM. The vectors reveal the posteriorly directed motion of the DM and swirls of cells moving from the medial to lateral PZ (Fig. 2A; supplementary material Fig. S3A-D). A similar swirling pattern is observed in the tailbud of avian embryos (Bénazéraf et al., 2010; Zamir et al., 2006). This flow pattern in the zebrafish PZ was also visualized by displaying the top 10% of tracks with the largest displacement in each direction (Fig. 2D,G; supplementary material Fig. S4A-D). Here, the ventral migration from the DM into the PZ was highlighted in the medial-posterior tailbud. This flow is segregated from the dorsal and anterior migration of the lateral periphery. We used finite element method (FEM) to quantify local rotational velocity within the flow field defined by the trajectories of the cell nuclei (Kelley and Ouellette, 2011). The rotation is displayed similarly to the velocity field, but the heat map indicates the magnitude of the local rotation and the arrows represent the projection of vorticity vectors. The direction of the arrows is perpendicular to the plane of rotation via the ‘right-hand rule’. A dorsal-to-ventral rotation exists within the DM and medial PZ (Fig. 2J; supplementary material Fig. S5A-D).

A transition from effective and coherent cell flow as cells move from the DM to the PZ

To examine local tissue motion, we averaged cell velocities over different radii (5, 10, 15, 20, 25, 30, 35, 40 μm) and displayed the velocity in a vector map. The map averaged over the 15 μm radius is representative and is shown next to the cell velocity vector map of the raw data (Fig. 3A,B). We then subtracted the average tissue motion from the individual tracks to display cell velocity variation from the local tissue average (Fig. 3C). This analysis demonstrated that local tissue motion in the PSM is small compared with local

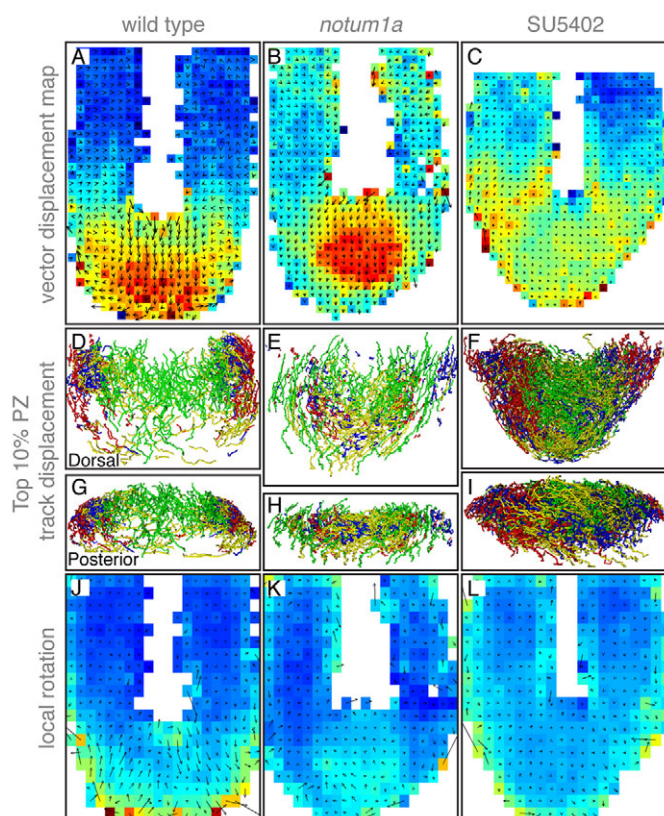


Fig. 2. Cell flow in the zebrafish tailbud. Wild-type (A,D,G,J), *notum1a*-overexpressing (B,E,H,K) and SU5402-treated (C,F,I,L) embryos. (A-C) The vector displacement map averages cell motion in discrete sectors. The heat map indicates mean speed with warmer colors indicating higher speeds and arrows signifying averaged 3D velocity vectors. See also supplementary material Fig. S3. (D-I) The top 10% of individual PZ tracks exhibiting the greatest displacement in each direction (green, dorsal to ventral; yellow, medial to lateral; red, posterior to anterior; blue, ventral to dorsal). See also supplementary material Fig. S4. (J-L) 3D finite element method was used to measure the local rotation in the flow of cells. Arrows slanting rightward indicate a dorsal-to-ventral local rotation whereas leftward-slanting arrows signify a ventral-to-dorsal local rotation.

tissue motion in the DM (Fig. 3B). Cellular variation from local tissue movement was also low in the PSM, particularly relative to the PZ (Fig. 3C). These general patterns are present when averaging velocities at all radii. However, averaging over larger radii leads to artifacts as local velocities in the DM appear reduced owing to averaging with adjacent slower PSM cells. Thus, to quantitatively examine cell motion, we analyzed the DM, PZ and PSM tracks separately.

Time lapses of the entire developing embryo show that cells in a given somite, e.g. somite ten, do not move relative to the body axis. Rather, the posterior tip of the tailbud progressively extends away from somite ten (Karlstrom and Kane, 1996; Schröter et al., 2008). Our analysis of local average velocity found that the PSM also displayed relatively little movement (Fig. 3A,B). The lack of net displacement along the anterior-posterior axis in the anterior part of the PSM was also evident. Thus, we used the anterior 50 μm of the PSM as our frame of reference. We calculated the center of mass of the velocities of the bilateral halves of the anterior 50 μm of the PSM in our datasets for each time point and subtracted

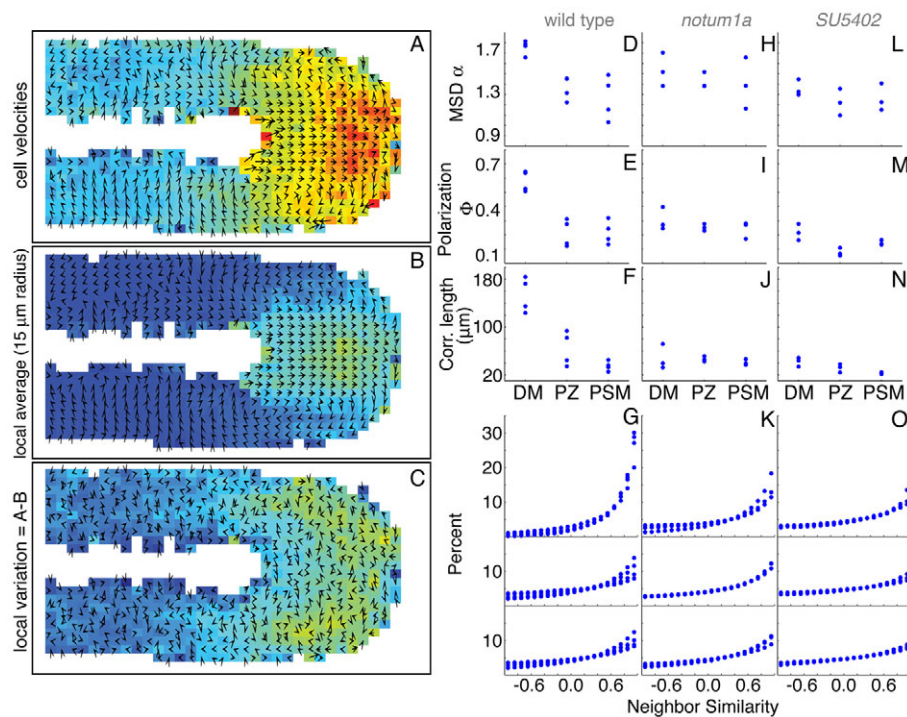


Fig. 3. Quantitative metrics reveal changes in tissue fluidity. (A) A vector map of cell velocities. Warmer colors represent higher velocities and arrows indicate the 2D projection of the averaged 3D velocity vectors. (B) A vector map of local tissue velocity averaged over a 15 μm radius. (C) A vector map of cell velocity variation from local tissue velocity. (D–O) Data for four wild-type zebrafish embryos (D–G), three *notum1a*-overexpressing embryos with elongation defects (H–K) and three SU5402-treated embryos with elongation defects (L–O). (D) The MSD exponent indicates that the movement is a combination of ballistic and Brownian motion for all regions with the DM being the most directed (DM vs PZ, $P < 0.05$; DM vs PSM, $P < 0.05$). Motion in the DM is strongly polarized (DM vs PZ, $P < 0.05$; DM vs PSM, $P < 0.05$) (E), has the largest length scale over which direction of motion is correlated (DM vs PZ, $P < 0.05$; DM vs PSM, $P < 0.05$) (F) and exhibits highest neighbor similarity (G). (H) MSD is not significantly changed in *notum1a*-overexpressing embryos (DM, $P > 0.05$). However, *notum1a* reduces the polarization ($P < 0.05$) (I), correlation length ($P < 0.05$) (J) and neighbor similarity (K) of the DM. (L) MSD in the DM is reduced in SU5402-treated embryos ($P < 0.05$). In addition, SU5402 treatment reduces the polarization ($P < 0.05$) (M), correlation length ($P < 0.05$) (N) and neighbor similarity (O) of the DM. P -values calculated using Student's t -test.

the movement of this center of mass from all other individual cell velocities for each time point. We used these relative velocities to calculate the value of the mean square displacement (MSD) exponent, polarization (Φ), correlation length of direction of motion, neighbor similarity, polar angle (ϕ), and convergence and extension as described below.

We calculated the MSD for each track and extracted the corresponding exponent values. An exponent value of 1 indicates pure diffusive motion and a value of 2 indicates ballistic motion. The data from four wild-type embryos were averaged for the DM, PZ and PSM. Cells in all three domains exhibited values between 1 and 2, indicative of directed migration (Fig. 3D). The DM exhibited a larger exponent value, consistent with it displaying the straightest and most rapid cell migration.

Neighbor similarity is a measure of the degree to which a cell migrates in the same direction as its immediate neighbors (Arboleda-Estudillo et al., 2010). The DM cells showed higher neighbor similarity than those of the PZ or PSM (Fig. 3G). We also quantified the global order in each domain via the polarization (Φ) which varies from 0 (disordered) to 1 (ordered) (Cavagna et al., 2010). The DM exhibited high polarization that was roughly twice that observed in the PZ or PSM, indicating that cells migrate more coherently in the DM (Fig. 3E). This loss of coherence as cells migrate into the PZ is reflected in the increase in the variation of individual cell motion relative to the local tissue motion in the PZ (Fig. 3C).

Lastly, we calculated the two-point correlation function of the normalized velocities (Angelini et al., 2010; Cavagna et al., 2010). As expected from the general geometry of the cell flow, the correlation length of the direction of motion was relatively high in the DM (~15 cell diameters) but dropped significantly as cells entered the PZ and remained low in the PSM (Fig. 3F).

Together, these data indicate that cell flow in the DM is rapid, ordered and posteriorly directed. As the cells enter the PZ, their speed is maintained but motion becomes less straight and less effective as migration loses much of its coherence and local coordination. Speed decreases as cells transition from the PZ to the PSM, and motion coherence continues to be low.

Reduction in Wnt signaling abrogates coherence of DM cell migration and bilateral symmetry in the PZ

The cell flow field analysis indicates that DM cells migrate coherently to the posterior end of the embryo where they adopt a less coordinated mode of cell migration. We found that this transition coincides with the expression of a number of Wnt inhibitors, including *notum1a* (Fig. 4C) (Flowers et al., 2012; Giráldez et al., 2002; Traister et al., 2008). *notum1a*, like a recently characterized planarian *notum* homolog, specifically inhibits canonical Wnt signaling and can do so when overexpressed during body elongation (Flowers et al., 2012;

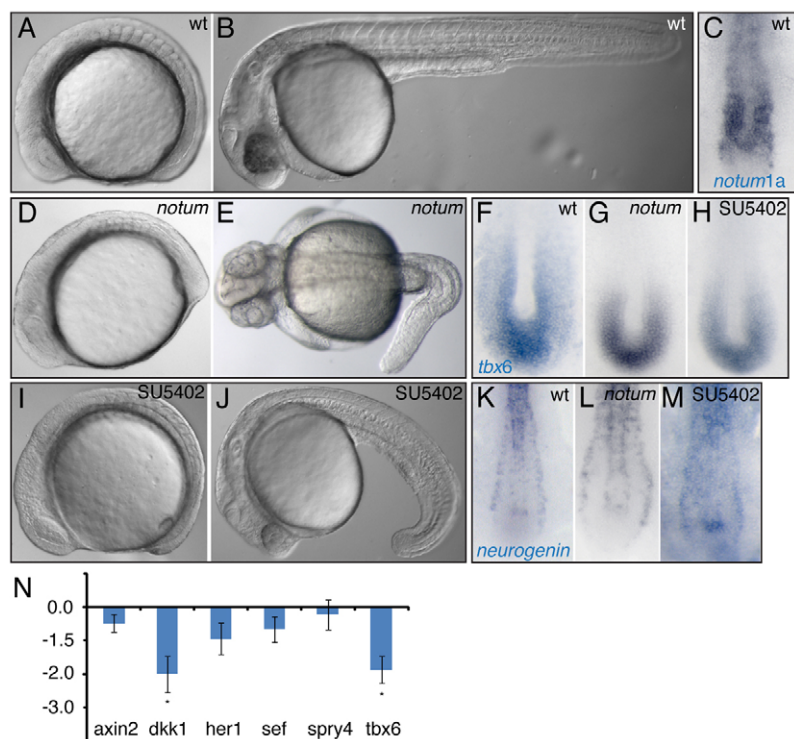


Fig. 4. Ectopic *notum1a* expression or SU5402 treatments perturb axis elongation. (A–M) Wild-type (A–C,F,K), *notum1a*-overexpressing (D,E,G,L) and SU5402-treated (H–J,M) zebrafish embryos. (C) *notum1a* is transcribed in the posterior DM. (D) Ectopic *notum1a* gives rise to a shortened axis and malformed tailbud. (E) Half of these embryos develop severely misdirected body axes. Spatial expression of *tbx6* (F–H) and *neurogenin1* (K–M) remains relatively normal despite *notum1a* overexpression (G,L) or SU5402 treatment (H,M). (I,J) SU5402 treatment gives rise to a mild axis elongation defect. (N) qPCR of dissected tailbuds after *notum1a* overexpression reveals reductions in transcription of *dkk1* and *tbx6*. Student's unpaired *t*-test. * $P \leq 0.05$. $n=4$. Error bars represent s.e.m.

Petersen and Reddien, 2011). Canonical Wnt signaling operates within a gene network required for zebrafish axis elongation, and we reasoned that *notum1a* might regulate cell migration in the tailbud (Shimizu et al., 2005; Szeto and Kimelman, 2004; Thorpe et al., 2005). We overexpressed *notum1a* by mRNA microinjection and observed axis elongation defects (Fig. 4D,E; supplementary material Fig. S6). We performed qPCR on pooled dissected tailbuds to assay for changes in canonical Wnt target gene and mesoderm specific transcription. Consistent with *notum1a* inhibiting Wnt signaling, we detected a strong reduction in expression of *dkk1*, a downstream target of canonical Wnt signaling, but not in expression of the Fgf targets *sef* (*ill17rd* – Zebrafish Information Network) and *sprouty4* (Fig. 4N) (Fürthauer et al., 2002; Fürthauer et al., 2001; Hashimoto et al., 2000; Shinya et al., 2000; Tsang et al., 2002). We also observed a significant reduction in *tbx6* expression suggesting a reduction in mesodermal cell fate. However, *in situ* hybridization for mesodermal markers such as *tbx6*, *her1* and *eve1* or the neural marker *neurogenin 1* suggests that the *notum1a* embryos with the misdirected body axes retain normally organized mesodermal and neural cell tissue (Fig. 4F,G,K,L; supplementary material Fig. S6) (Joly et al., 1993; Korzh et al., 1998).

Owing to difficulty imaging embryos with severely upturned body axes (supplementary material Fig. S6Q), we sorted eight-somite-stage *notum1a*-overexpressing embryos exhibiting mild elongation defects for time-lapse imaging (Fig. 4D). At the eight-somite stage, we have a 50% likelihood of identifying embryos that ultimately have elongation defects. Roughly half of the sorted embryos developed normal trunks and tails, whereas the other half exhibited misdirected trunks pointing dorsally, leftward or rightward (Fig. 4E; supplementary material Fig. S6). Accordingly, of the six *notum1a*-overexpressing embryos that we imaged, three had cell velocity fields similar to wild type whereas three were clearly abnormal. These latter three embryos displayed an obvious cell aggregation on the dorsal tailbud. The abnormal embryos

exhibited no significant change in either track straightness or mean cell speeds (supplementary material Fig. S1E–G, Fig. S2E–G).

The effects of ectopic *notum1a* expression on cell motion can be seen in the asymmetries in vector maps (Fig. 2B; supplementary material Fig. S3E–G). The medial posterior tailbud still exhibited relatively rapid, posteriorly biased cell movement, but the bilateral swirls in the PZ were absent. Similarly, the top 10% track displacement shows that the ventral and dorso-anterior flows were no longer segregated and bilaterally symmetric (Fig. 2E,H; supplementary material Fig. S4E–G). The vorticity vector map reveals that the dorsal-ventral local rotation in the flow field was disrupted and, in some cases, even reversed exhibiting ventral to dorsal rotation (Fig. 2K; supplementary material Fig. S5E–G).

These *notum1a*-overexpressing embryos showed no significant alteration in the value of the MSD exponent (Fig. 3H). However, when we examined the effects of *notum1a* overexpression on cell motion in the DM, we observed reduced neighbor similarity (Fig. 3K), polarization (Φ) (Fig. 3I) and correlation length of the direction of motion (Fig. 3J). The PZ and PSM were not significantly affected (Fig. 3H–K).

We also used a heat-shock dominant-negative Tcf-GFP transgenic zebrafish line (hs Δ TCF-GFP) to inhibit canonical Wnt signaling (Lewis et al., 2004). Heat shock of this line at the two-somite stage resulted in more severe abrogation of development than did injection of *notum1a* mRNA (Yin et al., 2011), and exhibited more severe quantitative effects on cell motion (supplementary material Fig. S7). Together, these data suggest that inhibition of canonical Wnt signaling in the tailbud reduces the coherence of migration in the DM.

Inhibition of Fgf signaling reduces DM cell migration coherence but not bilateral symmetry in the PZ

To examine Fgf signaling in the zebrafish tailbud, we performed a series of time-resolved perturbations with the Fgfr antagonist

SU5402 and quantified the onset of inhibition. We measured phosphorylation levels of the effectors Erk and Akt by western blot, and transcription of the direct Fgf targets *sprouty4* and *sef* by qPCR. We observed notable signal reduction in pooled dissected tailbuds after three hours treatment with SU5402 (Stulberg et al., 2012). This treatment led to a much milder effect on axis elongation than did *notum1a* inhibition of Wnt signaling (Fig. 4I,J). No bump formed in the DM and trunk elongation was linear. However, the embryos were shorter than normal and frequently displayed a kink in the posterior tail. Like *notum1a*-overexpressing embryos, these SU5402-treated embryos have relatively normal patterns of mesodermal and neural gene expression (Fig. 4H,M) (Stulberg et al., 2012).

To examine the role of Fgfr signaling in regulating cell flow within the tailbud, we began 4D confocal time-lapse analysis three hours after SU5402 treatment and imaged six embryos. As with half of the *notum1a*-overexpressing embryos, three of the SU5402-treated embryos were wild type in their quantitative cell flow metrics (not shown). However, the other three embryos exhibited changes in the DM that were equal to or stronger than the alterations seen in embryos with ectopic *notum1a*, and the alteration in cell flow is visually obvious. Cell track mean speed was unchanged in the DM (supplementary material Fig. S2), but the CV of track mean speed was modestly increased in both the DM and PZ (data not shown). Examination of polarization (Φ), correlation length of the direction of motion and neighbor similarity revealed reductions in the DM in line with those observed after *notum1a* overexpression (Fig. 3M-O). Thus, the coherence of migration was significantly reduced. Inhibition of Fgfr signaling

also strongly decreased the value of the MSD exponent and track straightness in the DM (Fig. 3L; supplementary material Fig. S1H-J). By comparison, track straightness was only weakly affected and the value of the MSD exponent was not changed by *notum1a* overexpression, suggesting that SU5402 treatment has a more robust effect on DM cell flow. Unlike *notum1a* overexpression, the SU5402 treatment caused neither a loss of bilateral symmetry in the flow pattern of the posterior tailbud (Fig. 2C,F,I; supplementary material Fig. S3H-J, Fig. S4H-J) nor a reversal in local rotational velocity (Fig. 2L; supplementary material Fig. S5H-J). Thus, whereas Fgfr inhibition more strongly affected quantitative metrics of cell flow in the DM, ectopic *notum1a*-overexpressing embryos displayed more dramatic alterations in dorsal-to-ventral rotation and bilateral symmetry of flow in the PZ and in overall axis morphology.

Tissue fluidity is regulated by Cadherin 2

cadherin 2 (*cdh2*) is required for normal tailbud morphology and axis elongation but not tailbud differentiation (Hammerschmidt et al., 1996; Harrington et al., 2007; Lele et al., 2002; Warga and Kane, 2007) (Fig. 5A,B). We examined cell flow in *cdh2*-null mutants to determine whether tissue fluidity was affected in ways that paralleled abrogation of Wnt or Fgf signaling. The *cdh2* mutant exhibited many of the same changes in cell motion but, overall, the effects on the quantitative metrics were stronger than those observed after either *notum1a* overexpression or SU5402 treatment (Fig. 5C-J). Loss of *cdh2* reduced the MSD exponent in the DM (Fig. 5G). The *cdh2* mutants also displayed reduction of the correlation length of the direction of motion both in the DM

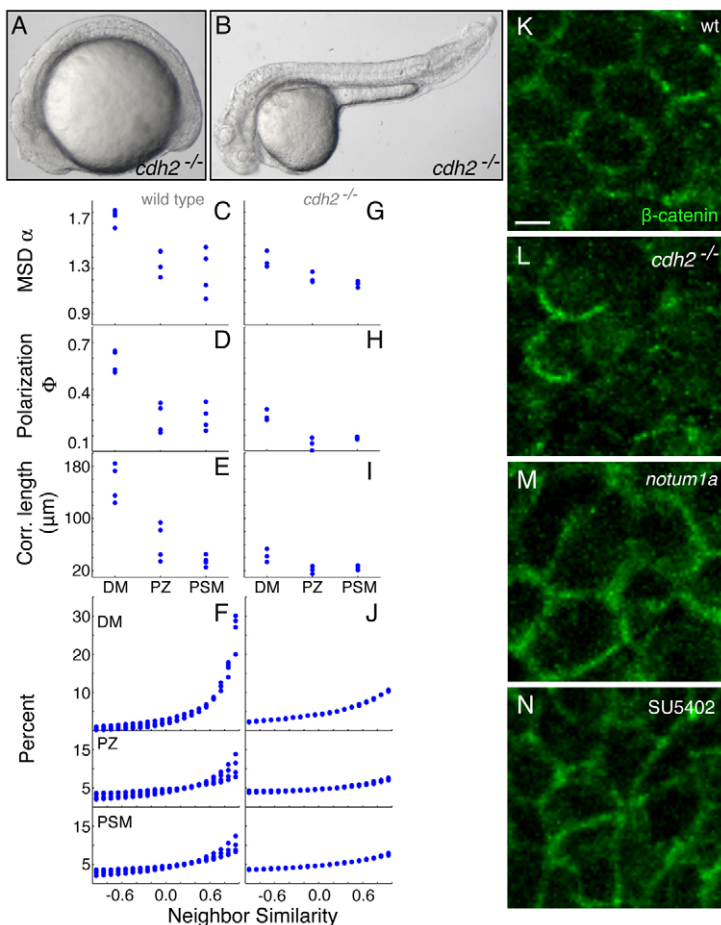


Fig. 5. Loss of *cadherin 2* reduces the effectiveness and coherence of cell motion in the zebrafish tailbud.

(A,B) *cdh2* mutants have morphologically abnormal tailbuds (A) and tails (B). (C-J) Quantitative analysis of cell motion in the tailbud of three wild-type embryos (C-F) and three *cdh2* mutants (G-J). (G) MSD is reduced in the DM of *cdh2* mutants ($P < 0.05$). (H) Polarization is reduced in the DM ($P < 0.05$), PZ ($P < 0.05$) and PSM ($P < 0.05$) of *cdh2* mutants. (I) Correlation length is lower in the DM ($P < 0.05$). (J) Neighbor similarity is diminished in the DM of *cdh2* homozygotes. (K-N) Adherens junctions in the PZ are visualized by immunohistochemistry for β -catenin. All panels are at the same magnification; scale bar: 5 μm . The lattice of adherens junctions among cells is present in wild-type embryos (K) but is disrupted in *cdh2* mutants (L). The pattern of adherens junctions in *notum1a*-overexpressing embryos (M) and SU5402-treated embryos (N) resembles the wild-type pattern. P -values calculated via Student's t -test.

and PZ (Fig. 5I) and reduction of polarization (Φ) in all domains (Fig. 5H). We wondered whether abrogation of either Wnt or Fgf signaling could be affecting cell flow via partial diminution of Cadherin-dependent cell adhesion. Thus, we examined adherens junctions by immunohistochemistry for β -catenin. In wild-type tailbuds, visualization of β -catenin revealed a lattice of adherens junctions (Fig. 5K), and this lattice was blotchy in *cdh2* mutants (Fig. 5L). However, we observed no obvious loss of adherens junctions in either *notum1a*-overexpressing or SU5402-treated tailbuds (Fig. 5M,N). These data suggest that reduction of Wnt or Fgf signaling in the tailbud does not primarily affect tissue fluidity by reducing Cadherin-dependent cell adhesion.

The balance between the coherence and rate of cell flow determines axis morphology

Inhibition of both Wnt and Fgf signaling reduced the coherence of cell flow in the DM, but ultimately had different effects on trunk elongation. To explore further the dynamics of cell flow in the tailbud, we studied a 2D model of self-propelled motion similar to a model used previously to study the emergence of order in cellular migration (Szabó et al., 2006). For simplicity, the tailbud is modeled as a ‘T’ geometry in 2D with reflective boundaries (Fig. 6; supplementary material Fig. S8 and Appendix S1). The bottom of the ‘T’ is anterior and the top is posterior. The upper portion of the vertical column represents the DM whereas the intersection with the vertical and horizontal sections is the PZ. Cells are introduced at the bottom of the ‘T’ at a constant rate and flow upward through the left and right ends of the top of the ‘T’. In the model, two forces determine the motion of a cell at each time point: a self-propulsion of constant magnitude and the force resulting from interactions with the neighbors or the walls of the ‘T’ (supplementary material Fig. S8

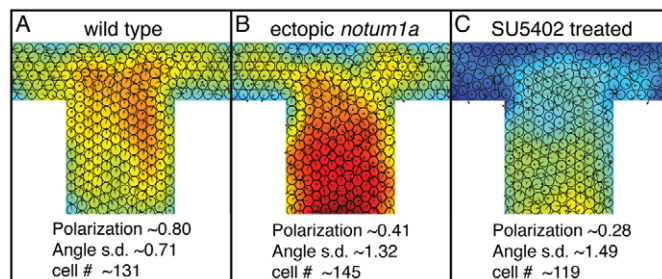


Fig. 6. Simulation of cell flow during trunk elongation.

(A–C) Sample snapshots of cell positions obtained using computer simulations of a 2D model system of self-propelled particles with soft interactions. The upper portion of the vertical column of the ‘T’ represents the DM whereas the intersection between the vertical and horizontal sections is representative of the PZ. Arrows denote the instantaneous velocity of each cell. Cell density is displayed as a heat map with warmer colors indicating higher density. See also supplementary material Fig. S8. (A) Wild-type simulation. (B) In ectopic *notum1a* embryos, cells are introduced at the lower column at the same rate as in wild type, but ectopic *notum1a* causes cells to move with higher angular noise (now the same as that of the PZ). (C) To model inhibition of Fgfr signaling by SU5402 treatment, the rate of addition of cells to the lower column is reduced to half the rate in A and B. Cells move with same randomness as in the ectopic *notum1a* embryos, but the attenuated cell flow into the DM reduces the number of cells in the DM. The polarization (Φ), standard deviation (std) of angles of posterior migration and cell number of the DM (vertical column) are the averages from 100 simulations for each of the three conditions.

and Appendix S1). The direction of the self-propulsion changes over time: it tends to align itself along the direction of motion but also experiences random fluctuations. To mimic the measured change in the coordination of cell motion at the DM-to-PZ transition, the noise in the angular alignment was set to be higher at the top of the ‘T’. This simulation produces a steady bilaterally symmetric flow, as observed in wild-type embryos (Fig. 6A). When instead noise in the angular alignment of the individual cells is increased throughout the vertical portion of the ‘T’, the flow becomes jammed (Fig. 6B). In the real embryo, we would expect such a jam to lead to expansion in the vertical direction (formation of a bump) or deviation of the tail axis. In the 2D simulation, jamming causes an accumulation of cells in the DM (Fig. 6B). However, unlike the posterior jam that forms after ectopic *notum1a* expression, the jams in the simulation form anywhere along the vertical portion of the ‘T’. Further simulations indicated that localization of cell aggregation to the top of the ‘T’ requires the noise in the angular alignment of the individual cells to be lower at the bottom of the ‘T’ than at the top. The prediction is that cells anterior to the DM, in what we call the anterior dorsal medial zone (ADM), should be more ordered than in the DM in *notum1a*-overexpressing tailbuds.

We compared the polarization (Φ) in the ADM and DM of three wild-type embryos, three *notum1a*-overexpressing embryos and three SU5402-treated embryos (Fig. 7A–C). In wild type, the polarization in both the ADM and DM was high (Fig. 7A). In embryos ectopically expressing *notum1a*, the ADM is always more ordered than the DM (Fig. 7B), which is consistent with the cell aggregation forming in the DM instead of the ADM as suggested by the simulations.

In the SU5402-treated embryos, the MSD exponent in the DM was decreased relative to wild type (Fig. 3D,L). This decline in effective migration in SU5402-treated embryos suggests an explanation for the different morphological phenotypes of *notum1a* and SU5402-treated embryos. In simulations, an increase in the disorder can be counterbalanced by a reduction in the flux of cells into the DM (Fig. 6C). This latter reduction curtails formation of jams in the flow (Fig. 6C) and bilateral flow is maintained. We examined posterior flow by calculating the medial-lateral angle of cell movement relative to direct posterior migration for each cell at each time point. The variability of posterior migration was calculated as the standard deviation of the polar angle (ϕ) distributions for the ADM and DM (Fig. 7D–F). In wild-type embryos, the angles tightly clustered near direct posterior migration. The distribution was broadest in SU5402-treated embryos. Thus, cells in the ADM and DM of SU5402-treated embryos were less posteriorly directed. The same trend is observed in the computer simulations (Fig. 6). The reduction in posteriorly directed migration was also evident in the effective migration of cells in the ADM and DM of SU5402-treated embryos. The MSD exponent of both domains was lower in SU5402-treated embryos, but not in *notum1a*-overexpressing embryos, relative to wild type (Fig. 7G–I). Lastly, we examined convergence towards the dorsal midline and extension along the anterior-posterior axis of the ADM and DM. We found that the ADM of SU5402-treated embryos displayed less extension than either wild-type or *notum1a*-overexpressing embryos (Fig. 7J–L). Thus, the flow of cells into the DM is lower after SU5402 treatment. These data, along with the simulations, suggest that the balance between the rate of cell flow and the coherence of the flow underpins the different elongation phenotypes in wild-type embryos, *notum1a*-overexpressing embryos and SU5402-treated embryos.

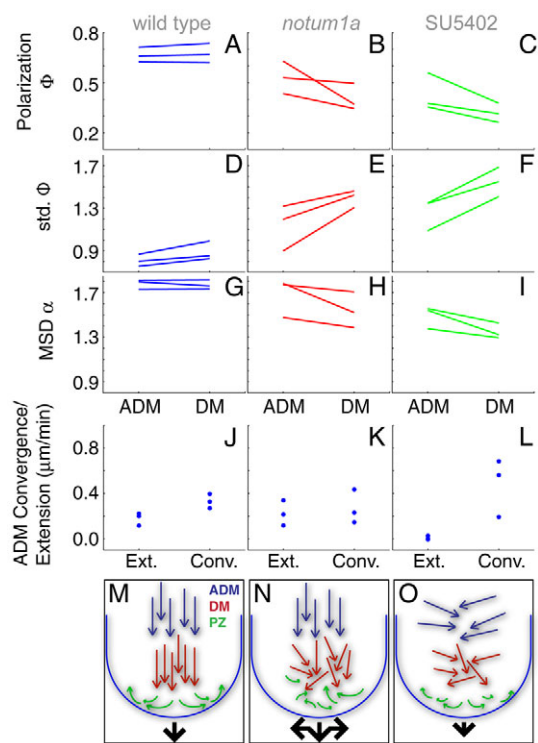


Fig. 7. Axis extension requires balance of cell flow rate and flow coherence. Wild-type (A,D,G,J,M), *notum1a*-overexpressing (B,E,H,K,N) and SU5402-treated (C,F,I,L,O) zebrafish embryos.

In A-I, values for ADM and DM are connected by a line, in order to compare the two domains in the same embryo. Thus, each line represents a single embryo. (A-C) Polarization (Φ). (D-F) Wild-type ADM and DM (D) show low variance in the angle of posterior migration (ϕ). The variance is not significantly changed in *notum1a*-overexpressing embryos (E) but the ADM variance is increased in SU5402-treated embryos (F) relative to wild type ($P < 0.05$), indicating progressively larger deviation from direct posterior migration. (G-I) The MSD is similarly high in the wild-type DM and ADM (G). *notum1a*-overexpressing DMs and ADMs have relatively high MSD, statistically indistinguishable from wild type, indicating continued effective migration (H). MSD is reduced in SU5402-treated embryos in the ADM compared with wild type ($P < 0.05$) (I). (J) The wild-type rate of ADM convergence and extension. (K,L) *notum1a*-overexpressing ADMs (K) display wild-type levels of convergence and extension, but SU5402-treated ADMs (L) show reduced extension ($P < 0.05$). *P*-values calculated using Student's *t*-test. (M) In wild type, a strong flow in the ADM and collective migration in the DM places cells at the posterior tip of the embryo. In the PZ, the coherence of the flow diminishes, which facilitates cell mixing and bilateral distribution of cells in the PZ. (N) In *notum1a*-overexpressing embryos, the coherence in the DM is prematurely lost but the flow rate in the ADM is maintained. Cells are unable to move through the tailbud and a 'traffic jam' forms leading to a bump and a turning of the axis. (O) In SU5402-treated embryos, the coherence in the DM is strongly reduced, as is the flux into the ADM. The latter reduction curtails the propensity of the flow to jam, thus cells pass through the PZ, albeit at a reduced rate, leading to a straight but shorter axis than that of wild type.

DISCUSSION

The data presented here show that neural and mesodermal progenitors dorsal to the neural tube exhibit highly ordered collective migration. As mesodermal precursors migrate ventrally at the posterior tip of the tailbud, the polarization (Φ), MSD exponent and neighbor similarity are reduced whereas average cell

velocity remains high. Cell labeling by two-photon laser uncaging indicates that neighboring cells in the DM become separated in the PZ and persist within the less coherent flow of the PZ for varying amounts of time before entering the PSM. This cell mixing promotes tissue homogenization, which is important as the new PZ cells express mesodermal and segmentation genes anew and need to synchronize their segmentation clocks with their neighbors (Uriu et al., 2010). Indeed, a remarkable feature of the posterior tailbud is the discrete domains of Wnt- and Fgf-dependent gene expression that persist despite extensive cell movement (Bénazéraf et al., 2010; Delfini et al., 2005; Mara et al., 2007; Zamir et al., 2006). As cells transition from the PZ to the PSM, the cell velocities decrease but the degree of order remains the same as in the PZ.

Complete inhibition of Fgf or Wnt signaling in zebrafish leads to severe axis truncation with loss of trunk and/or tail (Draper et al., 2003; Shimizu et al., 2005; Thorpe et al., 2005). We therefore examined relatively mild perturbations in these pathways in order to compare changes in cell movement with the normal flow observed in wild-type embryos. Both perturbations lead to a reduction in mesodermal gene expression, but the mild to undetectable effects on the spatial patterns of gene expression do not correlate with the strong changes in cell motion observed in the DM and ADM. Furthermore, examination of the *cdh2* mutant indicates that tissue fluidity can be similarly modified without affecting differentiation.

If cell motion in the DM were largely driven by bulk flow of the tissue, then a reduction in the polarization Φ should be accompanied by a decrease in cell velocity. However, *notum1a* overexpression and Fgfr inhibition affect the polarization Φ without reducing cell velocity, suggesting that the loss of coherence is instead due to alteration of self-propelled cell migration. The computer simulations demonstrate that increasing the angular noise in self-propelled cell motion reduces the polarization Φ , and these simulations are consistent with the phenotypes that are observed *in vivo*. In support of our conclusions, *in vitro* studies of traction and intercellular stresses in cell monolayers during collective cell migration do not support the idea that one group of cells produces compressive forces that push the cells at the leading edge. Rather, motion is driven by cooperative interactions between cells undergoing self-propelled migration (Treat and Fredberg, 2011).

The quantification of cell flow after *notum1a* overexpression and Fgfr inhibition shows that cell flow metrics show a complex relationship with the morphological phenotype. In ectopic *notum1a* embryos, cell flow in the DM is noisier than in wild-type embryos (Fig. 7M,N). The correlation length of direction of cell motion, polarization Φ and neighbor similarity are all diminished to levels normally seen in the PZ. However, the rate of posterior cell flow in the ADM remains high. Computer simulations suggest that this rapid, less organized flow results in a jam in the flow of the DM leading to bump formation, which resolves into bilaterally asymmetric flow. Fgfr inhibition leads to a reduction in coherence of the cell flow in the DM. But in contrast to *notum1a* overexpression, it also reduces the flux into the DM (Fig. 7O). Counter-intuitively, these more severe perturbations to the cell motion in the DM prevent cell aggregation, as the more slowly moving flow continues ventral rotation into the PZ and bilaterally symmetric distribution into the PSM.

An analogy to this cell flow can be made with automobile traffic on an expressway. When all vehicles travel at the same speed with no lane switching, as in wild-type coherent flow, then a high rate of travel can be stably maintained. However, when vehicles frequently switch lanes, as in the less coherent flow in ectopic

*notum*la-overexpressing embryos, then at high speed, accidents and traffic jams are inevitable. In the third situation, traffic is not coherent but the rate of cells entering the expressway is slower, as after Fgfr inhibition. Here, the slower addition of vehicles allows the traffic to continue to flow.

Acknowledgements

We thank Joe Wolenski for microscopy support; and Jamie Schwendinger-Schreck, Bryan Leland and Patrick McMillen for comments on the manuscript.

Funding

Research support was provided by a National Institutes of Health (NIH) predoctoral Developmental Biology training grant [T32 HD07180-29 to A.K.L.]; a NIH predoctoral Genetics training grant [T32 GM007499 to M.J.S.]; the National Institute of Child Health and Human Development (NICHD) [RO1 HD045738 to S.A.H.]; a Research Scholar Grant from the American Cancer Society [to S.A.H.]; the Raymond and Beverly Sackler Institute for Biological, Physical and Engineering Sciences [T.E. and S.A.H.]; the James McDonnell Foundation [T.E.]; and by the facilities and staff of the Yale University Faculty of Arts and Sciences High Performance Computing Center. Deposited in PMC for release after 12 months.

Competing interests statement

The authors declare no competing financial interests.

Supplementary material

Supplementary material available online at <http://dev.biologists.org/lookup/suppl/doi:10.1242/dev.090381/-DC1>

References

- Affolter, M., Zeller, R. and Caussinus, E. (2009). Tissue remodelling through branching morphogenesis. *Nat. Rev. Mol. Cell Biol.* **10**, 831-842.
- Amacher, S. L. and Kimmel, C. B. (1998). Promoting notochord fate and repressing muscle development in zebrafish axial mesoderm. *Development* **125**, 1397-1406.
- Angelini, T. E., Hannezo, E., Trepast, X., Fredberg, J. J. and Weitz, D. A. (2010). Cell migration driven by cooperative substrate deformation patterns. *Phys. Rev. Lett.* **104**, 168104.
- Arboleda-Estudillo, Y., Krieg, M., Stühmer, J., Licata, N. A., Muller, D. J. and Heisenberg, C. P. (2010). Movement directionality in collective migration of germ layer progenitors. *Curr. Biol.* **20**, 161-169.
- Bénazéraf, B., Francois, P., Baker, R. E., Denans, N., Little, C. D. and Pourquié, O. (2010). A random cell motility gradient downstream of FGF controls elongation of an amniote embryo. *Nature* **466**, 248-252.
- Bialek, W., Cavagna, A., Giardina, I., Mora, T., Silverstri, E., Viale, M. and Walczak, A. M. (2012). Statistical mechanics of natural flocks of birds. *Proc. Natl. Acad. Sci. USA* **113**, 4786-4791.
- Burnett, D. S. (1987). *Finite Element Analysis: From Concepts to Applications*. Reading, MA, USA: Addison-Wesley Publishing Co.
- Cavagna, A., Cimarelli, A., Giardina, I., Parisi, G., Santagati, R., Stefanini, F. and Viale, M. (2010). Scale-free correlations in starling flocks. *Proc. Natl. Acad. Sci. USA* **107**, 11865-11870.
- Delfini, M. C., Dubrulle, J., Malapert, P., Chal, J. and Pourquié, O. (2005). Control of the segmentation process by graded MAPK/ERK activation in the chick embryo. *Proc. Natl. Acad. Sci. USA* **102**, 11343-11348.
- Draper, B. W., Morcos, P. A. and Kimmel, C. B. (2001). Inhibition of zebrafish fgf8 pre-mRNA splicing with morpholino oligos: a quantifiable method for gene knockdown. *Genesis* **30**, 154-156.
- Draper, B. W., Stock, D. W. and Kimmel, C. B. (2003). Zebrafish fgf24 functions with fgf8 to promote posterior mesodermal development. *Development* **130**, 4639-4654.
- Dubrulle, J., McGrew, M. J. and Pourquié, O. (2001). FGF signaling controls somite boundary position and regulates segmentation clock control of spatiotemporal Hox gene activation. *Cell* **106**, 219-232.
- Dunty, W. C., Jr, Biris, K. K., Chalamalasetty, R. B., Taketo, M. M., Lewandoski, M. and Yamaguchi, T. P. (2008). Wnt3a/beta-catenin signaling controls posterior body development by coordinating mesoderm formation and segmentation. *Development* **135**, 85-94.
- Flowers, G. P., Topczewska, J. M. and Topczewski, J. (2012). A zebrafish Notum homolog specifically blocks the Wnt/ β -catenin signaling pathway. *Development* **139**, 2416-2425.
- Fürthauer, M., Reifers, F., Brand, M., Thisse, B. and Thisse, C. (2001). sprouty4 acts in vivo as a feedback-induced antagonist of FGF signaling in zebrafish. *Development* **128**, 2175-2186.
- Fürthauer, M., Lin, W., Ang, S. L., Thisse, B. and Thisse, C. (2002). Sef is a feedback-induced antagonist of Ras/MAPK-mediated FGF signalling. *Nat. Cell Biol.* **4**, 170-174.
- Giráldez, A. J., Copley, R. R. and Cohen, S. M. (2002). HSPG modification by the secreted enzyme Notum shapes the Wingless morphogen gradient. *Dev. Cell* **2**, 667-676.
- Griffin, K. J. and Kimelman, D. (2002). One-Eyed Pinhead and Spadetail are essential for heart and somite formation. *Nat. Cell Biol.* **4**, 821-825.
- Griffin, K. J. and Kimelman, D. (2003). Interplay between FGF, one-eyed pinhead, and T-box transcription factors during zebrafish posterior development. *Dev. Biol.* **264**, 456-466.
- Griffin, K. J., Amacher, S. L., Kimmel, C. B. and Kimelman, D. (1998). Molecular identification of spadetail: regulation of zebrafish trunk and tail mesoderm formation by T-box genes. *Development* **125**, 3379-3388.
- Griffith, C. M., Wiley, M. J. and Sanders, E. J. (1992). The vertebrate tail bud: three germ layers from one tissue. *Anat. Embryol. (Berl.)* **185**, 101-113.
- Hammerschmidt, M., Pelegri, F., Mullins, M. C., Kane, D. A., Brand, M., van Eeden, F.-J., Furutani-Seiki, M., Granato, M., Haffter, P., Heisenberg, C.-P. et al. (1996). Mutations affecting morphogenesis during gastrulation and tail formation in the zebrafish, *Danio rerio*. *Development* **123**, 143-151.
- Harrington, M. J., Hong, E., Fasanmi, O. and Brewster, R. (2007). Cadherin-mediated adhesion regulates posterior body formation. *BMC Dev. Biol.* **7**, 130.
- Harrington, M. J., Chalasani, K. and Brewster, R. (2010). Cellular mechanisms of posterior neural tube morphogenesis in the zebrafish. *Dev. Dyn.* **239**, 747-762.
- Hashimoto, H., Itoh, M., Yamanaka, Y., Yamashita, S., Shimizu, T., Solnica-Krezel, L., Hibi, M. and Hirano, T. (2000). Zebrafish Dkk1 functions in forebrain specification and axial mesoderm formation. *Dev. Biol.* **217**, 138-152.
- Heisenberg, C. P. and Solnica-Krezel, L. (2008). Back and forth between cell fate specification and movement during vertebrate gastrulation. *Curr. Opin. Genet. Dev.* **18**, 311-316.
- Holley, S. A., Geisler, R. and Nüsslein-Volhard, C. (2000). Control of her1 expression during zebrafish somitogenesis by a delta-dependent oscillator and an independent wave-front activity. *Genes Dev.* **14**, 1678-1690.
- Holmdahl, D. E. (1925). Experimentelle Untersuchungen über die Lage der Grenze primärer und sekundärer Körperentwicklung beim Huhn. *Anat. Anz.* **59**, 393-396.
- Joly, J. S., Joly, C., Schulte-Merker, S., Boulekbache, H. and Combamine, H. (1993). The ventral and posterior expression of the zebrafish homeobox gene *eve1* is perturbed in dorsalized and mutant embryos. *Development* **119**, 1261-1275.
- Jülich, D., Geisler, R., Tübingen 2000 Screen Consortium and Holley, S. A. (2005). Integrin α 5 and delta/notch signaling have complementary spatiotemporal requirements during zebrafish somitogenesis. *Dev. Cell* **8**, 575-586.
- Jülich, D., Mould, A. P., Koper, E. and Holley, S. A. (2009). Control of extracellular matrix assembly along tissue boundaries via Integrin and Eph/Ephrin signaling. *Development* **136**, 2913-2921.
- Kanki, J. P. and Ho, R. K. (1997). The development of the posterior body in zebrafish. *Development* **124**, 881-893.
- Karlstrom, R. O. and Kane, D. A. (1996). A flipbook of zebrafish embryogenesis. *Development* **123**, 461.
- Kawamura, A., Koshida, S. and Takada, S. (2008). Activator-to-repressor conversion of T-box transcription factors by the Ripply family of Groucho/TLE-associated mediators. *Mol. Cell. Biol.* **28**, 3236-3244.
- Keegan, B. R., Feldman, J. L., Lee, D. H., Koos, D. S., Ho, R. K., Stainier, D. Y. and Yelon, D. (2002). The elongation factors Pandora/Spt6 and Foggy/Spt5 promote transcription in the zebrafish embryo. *Development* **129**, 1623-1632.
- Keller, P. J., Schmidt, A. D., Wittbrodt, J. and Stelzer, E. H. (2008). Reconstruction of zebrafish early embryonic development by scanned light sheet microscopy. *Science* **322**, 1065-1069.
- Kelley, D. H. and Ouellette, N. T. (2011). Onset of three-dimensionality in electromagnetically driven thin-layer flows. *Phys. Fluids* **23**, 045103.
- Kimelman, D. (2006). Mesoderm induction: from caps to chips. *Nat. Rev. Genet.* **7**, 360-372.
- Korzh, V., Sleptsova, I., Liao, J., He, J. and Gong, Z. (1998). Expression of zebrafish bHLH genes *ngn1* and *nrd* defines distinct stages of neural differentiation. *Dev. Dyn.* **213**, 92-104.
- Lee, D. T. and Schachter, B. J. (1980). Two algorithms for constructing a delaunay triangulation. *Int. J. Comput. Information Sci.* **9**, 219-242.
- Lele, Z., Folchert, A., Concha, M., Rauch, G. J., Geisler, R., Rosa, F., Wilson, S. W., Hammerschmidt, M. and Bally-Cuif, L. (2002). parachute/n-cadherin is required for morphogenesis and maintained integrity of the zebrafish neural tube. *Development* **129**, 3281-3294.
- Lewis, J. L., Bonner, J., Modrell, M., Ragland, J. W., Moon, R. T., Dorsky, R. I. and Raible, D. W. (2004). Reiterated Wnt signaling during zebrafish neural crest development. *Development* **131**, 1299-1308.
- Liu, M. B. and Liu, G. R. (2010). Smoothed particle hydrodynamics (SPH): an overview and recent developments. *Arch. Comput. Method. E* **17**, 25-76.
- Liu, M. B., Liu, G. R. and Lam, K. Y. (2003). Constructing smoothing functions in smoothed particle hydrodynamics with applications. *J. Comput. Appl. Math.* **155**, 263-284.

- Mara, A., Schroeder, J., Chalouni, C. and Holley, S. A. (2007). Priming, initiation and synchronization of the segmentation clock by deltaD and deltaC. *Nat. Cell Biol.* **9**, 523-530.
- Marlow, F., Gonzalez, E. M., Yin, C., Rojo, C. and Solnica-Krezel, L. (2004). No tail co-operates with non-canonical Wnt signaling to regulate posterior body morphogenesis in zebrafish. *Development* **131**, 203-216.
- Martin, B. L. and Kimelman, D. (2008). Regulation of canonical Wnt signaling by Brachyury is essential for posterior mesoderm formation. *Dev. Cell* **15**, 121-133.
- Martin, B. L. and Kimelman, D. (2012). Canonical Wnt signaling dynamically controls multiple stem cell fate decisions during vertebrate body formation. *Dev. Cell* **22**, 223-232.
- Mathis, L., Kulesa, P. M. and Fraser, S. E. (2001). FGF receptor signalling is required to maintain neural progenitors during Hensen's node progression. *Nat. Cell Biol.* **3**, 559-566.
- Mohammadi, M., McMahon, G., Sun, L., Tang, C., Hirth, P., Yeh, B. K., Hubbard, S. R. and Schlessinger, J. (1997). Structures of the tyrosine kinase domain of fibroblast growth factor receptor in complex with inhibitors. *Science* **276**, 955-960.
- Monaghan, J. J. (1992). Smoothed particle hydrodynamics. *Annu. Rev. Astron. Astr.* **30**, 543-574.
- Naiche, L. A., Holder, N. and Lewandoski, M. (2011). FGF4 and FGF8 comprise the wavefront activity that controls somitogenesis. *Proc. Natl. Acad. Sci. USA* **108**, 4018-4023.
- Niwa, Y., Masamizu, Y., Liu, T., Nakayama, R., Deng, C. X. and Kageyama, R. (2007). The initiation and propagation of Hes7 oscillation are cooperatively regulated by Fgf and notch signaling in the somite segmentation clock. *Dev. Cell* **13**, 298-304.
- Nüsslein-Volhard, C. and Dahm, R. (2002). *Zebrafish*. Oxford, UK: Oxford University Press.
- Okuda, Y., Ogura, E., Kondoh, H. and Kamachi, Y. (2010). B1 SOX coordinate cell specification with patterning and morphogenesis in the early zebrafish embryo. *PLoS Genet.* **6**, e1000936.
- Olivier, N., Luengo-Oroz, M. A., Duloquin, L., Faure, E., Savy, T., Veilleux, I., Solinas, X., Débarre, D., Bourguine, P., Santos, A. et al. (2010). Cell lineage reconstruction of early zebrafish embryos using label-free nonlinear microscopy. *Science* **329**, 967-971.
- Park, W. Y., Miranda, B., Lebeche, D., Hashimoto, G. and Cardoso, W. V. (1998). FGF-10 is a chemotactic factor for distal epithelial buds during lung development. *Dev. Biol.* **201**, 125-134.
- Petersen, C. P. and Reddien, P. W. (2011). Polarized notum activation at wounds inhibits Wnt function to promote planarian head regeneration. *Science* **332**, 852-855.
- Pourquié, O. (2011). Vertebrate segmentation: from cyclic gene networks to scoliosis. *Cell* **145**, 650-663.
- Quesada-Hernández, E., Caneparo, L., Schneider, S., Winkler, S., Lieblich, M., Fraser, S. E. and Heisenberg, C. P. (2010). Stereotypical cell division orientation controls neural rod midline formation in zebrafish. *Curr. Biol.* **20**, 1966-1972.
- Rauch, G.-J., Granato, M. and Haffter, P. (1997a). A polymorphic zebrafish line for genetic mapping using SSLPs on high-percentage agarose gels. *Tech. Tips Online* **2**, 145-147.
- Rauch, G. J., Hammerschmidt, M., Blader, P., Schauerte, H. E., Strähle, U., Ingham, P. W., McMahon, A. P. and Haffter, P. (1997b). Wnt5 is required for tail formation in the zebrafish embryo. *Cold Spring Harb. Symp. Quant. Biol.* **62**, 227-234.
- Roszko, I., Sawada, A. and Solnica-Krezel, L. (2009). Regulation of convergence and extension movements during vertebrate gastrulation by the Wnt/PCP pathway. *Semin. Cell Dev. Biol.* **20**, 986-997.
- Row, R. H. and Kimelman, D. (2009). Bmp inhibition is necessary for post-gastrulation patterning and morphogenesis of the zebrafish tailbud. *Dev. Biol.* **329**, 55-63.
- Russek-Blum, N., Nabel-Rosen, H. and Levkowitz, G. (2010). Two-photon-based photoactivation in live zebrafish embryos. *J. Vis. Exp.* **46**, 1902.
- Sawada, A., Shinya, M., Jiang, Y. J., Kawakami, A., Kuroiwa, A. and Takeda, H. (2001). Fgf/MAPK signalling is a crucial positional cue in somite boundary formation. *Development* **128**, 4873-4880.
- Schröter, C., Herrgen, L., Cardona, A., Brouhard, G. J., Feldman, B. and Oates, A. C. (2008). Dynamics of zebrafish somitogenesis. *Dev. Dyn.* **237**, 545-553.
- Shimizu, T., Bae, Y. K., Muraoka, O. and Hibi, M. (2005). Interaction of Wnt and caudal-related genes in zebrafish posterior body formation. *Dev. Biol.* **279**, 125-141.
- Shinya, M., Eschbach, C., Clark, M., Lehrach, H. and Furutani-Seiki, M. (2000). Zebrafish Dkk1, induced by the pre-MBT Wnt signaling, is secreted from the prechordal plate and patterns the anterior neural plate. *Mech. Dev.* **98**, 3-17.
- Shirasaki, R., Lewcock, J. W., Lettieri, K. and Pfaff, S. L. (2006). FGF as a target-derived chemoattractant for developing motor axons genetically programmed by the LIM code. *Neuron* **50**, 841-853.
- Stoick-Cooper, C. L., Weidinger, G., Riehle, K. J., Hubbert, C., Major, M. B., Fausto, N. and Moon, R. T. (2007). Distinct Wnt signaling pathways have opposing roles in appendage regeneration. *Development* **134**, 479-489.
- Stulberg, M. J., Lin, A., Zhao, H. and Holley, S. A. (2012). Crosstalk between Fgf and Wnt signaling in the zebrafish tailbud. *Dev. Biol.* **369**, 298-307.
- Sun, X., Meyers, E. N., Lewandoski, M. and Martin, G. R. (1999). Targeted disruption of Fgf8 causes failure of cell migration in the gastrulating mouse embryo. *Genes Dev.* **13**, 1834-1846.
- Sutherland, D., Samakovlis, C. and Krasnow, M. A. (1996). branchless encodes a Drosophila FGF homolog that controls tracheal cell migration and the pattern of branching. *Cell* **87**, 1091-1101.
- Szabó, B., Szöllösi, G. J., Gönci, B., Jurányi, Z., Selmececi, D. and Vicsek, T. (2006). Phase transition in the collective migration of tissue cells: experiment and model. *Phys. Rev. E Stat. Nonlin. Soft Matter Phys.* **74**, 061908.
- Szeto, D. P. and Kimelman, D. (2004). Combinatorial gene regulation by Bmp and Wnt in zebrafish posterior mesoderm formation. *Development* **131**, 3751-3760.
- Takada, S., Stark, K. L., Shea, M. J., Vassileva, G., McMahon, J. A. and McMahon, A. P. (1994). Wnt-3a regulates somite and tailbud formation in the mouse embryo. *Genes Dev.* **8**, 174-189.
- Takemoto, T., Uchikawa, M., Yoshida, M., Bell, D. M., Lovell-Badge, R., Papaioannou, V. E. and Kondoh, H. (2011). Tbx6-dependent Sox2 regulation determines neural or mesodermal fate in axial stem cells. *Nature* **470**, 394-398.
- Thorpe, C. J., Weidinger, G. and Moon, R. T. (2005). Wnt/beta-catenin regulation of the Sp1-related transcription factor sp51 promotes tail development in zebrafish. *Development* **132**, 1763-1772.
- Traister, A., Shi, W. and Filmus, J. (2008). Mammalian Notum induces the release of glypicans and other GPI-anchored proteins from the cell surface. *Biochem. J.* **410**, 503-511.
- Treat, X. and Fredberg, J. J. (2011). Plithotaxis and emergent dynamics in collective cellular migration. *Trends Cell Biol.* **21**, 638-646.
- Tsang, M., Friesel, R., Kudoh, T. and Dawid, I. B. (2002). Identification of Sef, a novel modulator of FGF signalling. *Nat. Cell Biol.* **4**, 165-169.
- Tucker, J. A., Mintzer, K. A. and Mullins, M. C. (2008). The BMP signaling gradient patterns dorsoventral tissues in a temporally progressive manner along the anteroposterior axis. *Dev. Cell* **14**, 108-119.
- Tzouanacou, E., Wegener, A., Wymeersch, F. J., Wilson, V. and Nicolas, J. F. (2009). Redefining the progression of lineage segregations during mammalian embryogenesis by clonal analysis. *Dev. Cell* **17**, 365-376.
- Uriu, K., Morishita, Y. and Iwasa, Y. (2010). Random cell movement promotes synchronization of the segmentation clock. *Proc. Natl. Acad. Sci. USA* **107**, 4979-4984.
- Vicsek, T. and Zafeiris, A. (2012). Collective motion. *Physics Reports* **517**, 71-140.
- Wahl, M. B., Deng, C., Lewandoski, M. and Pourquié, O. (2007). FGF signaling acts upstream of the NOTCH and WNT signaling pathways to control segmentation clock oscillations in mouse somitogenesis. *Development* **134**, 4033-4041.
- Wallingford, J. B., Fraser, S. E. and Harland, R. M. (2002). Convergent extension: the molecular control of polarized cell movement during embryonic development. *Dev. Cell* **2**, 695-706.
- Warga, R. M. and Kane, D. A. (2007). A role for N-cadherin in mesodermal morphogenesis during gastrulation. *Dev. Biol.* **310**, 211-225.
- Weidinger, G., Thorpe, C. J., Wuennenberg-Stapleton, K., Ngai, J. and Moon, R. T. (2005). The Sp1-related transcription factors sp5 and sp5-like act downstream of Wnt/beta-catenin signaling in mesoderm and neuroectoderm patterning. *Curr. Biol.* **15**, 489-500.
- Wilson, V., Olivera-Martinez, I. and Storey, K. G. (2009). Stem cells, signals and vertebrate body axis extension. *Development* **136**, 1591-1604.
- Yang, X., Dormann, D., Münsterberg, A. E. and Weijer, C. J. (2002). Cell movement patterns during gastrulation in the chick are controlled by positive and negative chemotaxis mediated by FGF4 and FGF8. *Dev. Cell* **3**, 425-437.
- Yin, A., Korzh, S., Winata, C. L., Korzh, V. and Gong, Z. (2011). Wnt signaling is required for early development of zebrafish swimbladder. *PLoS ONE* **6**, e18431.
- Zamir, E. A., Czirók, A., Cui, C., Little, C. D. and Rongish, B. J. (2006). Mesodermal cell displacements during avian gastrulation are due to both individual cell-autonomous and convective tissue movements. *Proc. Natl. Acad. Sci. USA* **103**, 19806-19811.
- Zhang, Y., Yeh, J. R., Mara, A., Ju, R., Hines, J. F., Cirone, P., Griesbach, H. L., Schneider, I., Slusarski, D. C., Holley, S. A. et al. (2006). A chemical and genetic approach to the mode of action of fumagillin. *Chem. Biol.* **13**, 1001-1009.
- Zhang, L., Kendrick, C., Jülich, D. and Holley, S. A. (2008). Cell cycle progression is required for zebrafish somite morphogenesis but not segmentation clock function. *Development* **135**, 2065-2070.